CLUSTERING THE INFANT BRAIN TISSUES BASED ON MICROSTRUCTURAL PROPERTIES AND MATURATION ASSESSMENT USING MULTI-PARAMETRIC MRI

J. Lebenberg[1]*, C. Poupon*[2]*, B. Thirion*[3]*, F. Leroy*[1]*, J.-F. Mangin*[4]*, G. Dehaene-Lambertz*[1] *and J. Dubois*[1]

[1] INSERM-CEA, Neurospin Center, Cognitive Neuroimaging Unit U992, Gif-Sur-Yvette, France
[2] CEA, NeuroSpin Center, UNIRS, Gif-sur-Yvette, France
[3] INRIA, NeuroSpin Center, Parietal, Gif-sur-Yvette, France
[4] CEA, NeuroSpin Center, UNATI, Gif-sur-Yvette, France

ABSTRACT

Microstructural and physiological changes are intense in the developing brain, thus considerably modifying parameters quantified by MRI (relaxation times, anisotropy and diffusivities). The latest advances in EPI enabled to non-invasively measure these parameters in infants in a reasonable acquisition time to follow brain maturation. To take advantage of the parameters complementarity, we first proposed to correct EPI distortions by a registration approach never applied on infants' data. We then clustered brain regions according to their different microstructural properties and maturation, without spatial priors. Results were in agreement with *post-mortem* studies : maturation proceeds from center to periphery ; first maturing regions included primary regions, but also the amygdala and the medial cingular region. The most delayed regions were observed in superior frontal and parietal lobes. In future analyses, we will propose new partitions of the whole brain and of specific functional regions based on maturation patterns returned by this approach.

***Index Terms*—** Developing brain, EPI distortion, multimodal image registration, clustering

1. INTRODUCTION

During the first post-natal weeks, dendritic development and myelination are intense in the brain grey and white matters, occurring at different times and speeds according to brain regions and underlying networks. The reference works on this maturation progression remain the rare *post-mortem* studies that have reported asynchrony within the white matter and the cortical regions [1]. As these changes modify the molecules environment and restrict water movement in the developing cerebral tissues, parameters measured by magnetic resonance imaging (MRI) are consequently affected. In the infant brain, previous works have shown that these parameters, including quantitative relaxation times (qT1 and qT2) and parameters provided by diffusion tensor imaging (DTI : longitudinal diffusivity $\lambda_{//}$, transverse diffusivity $\lambda_{\perp}$ and fractional anisotropy imaging FA), can be used to differentiate the developing grey matter (GM) and the white matter (WM) myelinating fascicles [2]. All these MRI parameters are indeed sensitive to changes induced by maturation, but their maturational sensitivity is ought to differ in regards to their biophysical mechanisms [3]. Thus combining these parameters may better highlight the maturation asynchrony across brain regions than univariate analyses, as demonstrated for WM bundles [4]. Thanks to the latest advances in echo-planar imaging (EPI), quantitative mappings related to T1- and T2-relaxometries as well as DTI are available within a limited acquisition time, providing valuable information on the tissues organization and microstructure non-invasively in a few minutes and making their use reasonable in healthy infants [5]. However, EPI sequences suffer from distortions induced by magnetic field inhomogeneities all along the phase-encode direction and by large differences in magnetic susceptibility close to the interfaces between air, skull and brain. Precisely correcting for these distortions is thus essential to reliably superpose quantitative maps and anatomical images, especially for the cortex whose ribbon is very thin in the developing brain. Because of limited acquisition time in infants, the common approach used to correct these geometrical deformations, based on fieldmap calibration [6], could not be applied for all infants (these maps were not acquired because of time constraints). So we here proposed to directly register all distorted maps (qT1, qT2, DTI) on undistorted anatomical images [7, 8]. For the first time, this approach was applied on infants' data. We then investigated whether a clustering analysis [9] can provide a partition of developing tissues without any priors on spatial localization for regions of interest.

2. MATERIAL AND METHODS

2.1. Acquisition

The database included 17 sets of images obtained in spontaneously asleep healthy term-born infants, aged from 3 to 21 weeks (corrected ages for gestational age at birth), under a protocol approved by the Institutional Ethical Committee. Spin-echo EPI sequences (1.8mm isotropic) were acquired in less than 11min on a 3T MRI Trio system using a 32-channels head coil (Siemens HealthCare, Erlangen, Germany) and using the y-axis as the phase-encoding direction. For DTI, 30 diffusion gradient orientations were used at b=700s.mm^{-2}. For qT1 and qT2, 8 inversion times (TI : 250→2500ms) and 8 echo times (TE : 50→260ms) were used respectively. MRI parameters (FA, $\lambda_{//}$ and $\lambda_{\perp}$, qT1, qt2) were estimated in each voxel using the Connectomist and Relaxometrist toolboxes [10]. For each subject, anatomical T2-weighted images (T2w-MRI) were also acquired ($1\times1\times1.1$mm^3) using a turbo spin-echo sequence.

The research leading to these results has received funding from the European Union Seventh Framework Programme (FP7/2007-2013) under grant agreement no. 604102 (Human Brain Project). MRI acquisitions have been financed thanks to Fyssen Foundation.

2.2. Distortion correction and multimodal image registration

To be able to reliably compare the parameter maps in particular in voxels located in the cortex whose thickness may be less than 2mm in infants, the first step was to correct geometrical distortions due to the use of EPI read echotrains. We proposed to correct distortions by directly registering, one after the other, the resulting qT1, qT2 and $\lambda_{//}$ maps with the subject's T2w-MRI [7, 8]. Resulting from the same acquisition, $\lambda_{\perp}$ and FA maps were deformed using the transformation estimated on $\lambda_{//}$ maps.

A global rigid transformation based on mutual information (MI) was first estimated between the brains semi-automatically extracted from the quantitative images and the one semi-automatically extracted from the corresponding anatomical image [11]. An elastic deformation, based on cubic B-splines and using MI as a similarity criterion, was then estimated for each quantitative image to locally improve the correction [12]. This algorithm uses coarse-to-fine uniformed 3D grids of control points to locally estimate the registration. Adult brain studies based on a similar approach often limited their deformation along the phase-encode direction [8]. Here a supplementary difficulty relied on the position of the baby's head inside the MR scanner (because the babies were spontaneously asleep, it was not possible to get their head perfectly aligned with MR axes, so frontal sinuses were not on a sole axis on EPI images). Moreover, the infant brain is not perfectly centered into the skull : the distance between brain and skull can be very thin (cf. **Fig.1a)**, yellow arrows and [13]) and can thus adding distortions through any directions. Contrary to recommendations previously made for adults studies, the elastic deformation was consequently estimated on all directions.

For 4 infants with a regularly-spaced age (3w, 6w, 13w and 19w), manual landmarks were delineated on quantitative images before and after the non-linear registration, at the level of frontal and occipital lobes (where distortions were visually the most important) and on the lateral ventricles (to characterize a central region). In addition to visual assessments, the image registration was quantitatively evaluated by computing the Chamfer distances between these landmarks and similar marks fixed on anatomical images.

2.3. Clustering analysis

To classify tissues according to their different microstructural properties and their degree of maturation, a clustering analysis was performed from the registered MRI parameter maps (qT1, qT2, FA, $\lambda_{//}$ and $\lambda_{\perp}$) using Gaussian Mixture Modeling (10 initializations) based on an Expectation-Maximization algorithm (10 iterations) and using all brains together (i.e. 5 data $\times$ 17 infants). The CSF was previously automatically removed from the data using a histogram analysis.

For the clustering analysis, the number of classes was a required input parameter. We hypothesized that characterizing the developing tissues would require at least 7 classes in infants : immature GM, averagely mature GM, mature GM, immature WM non-compactly organized, immature WM compactly organized, mature WM non-compactly organized, and mature WM compactly organized. To validate this hypothesis, we expected to find known results : first mature WM and GM regions should be in central regions, and a progression in the maturation patterns should be observed with increasing age of the infants [1]. In addition, normalized volumes (defined as the volume of each class divided by the whole brain volume) were plotted as a function of age assuming that the volumes of immature classes should decrease with age while the reverse is expected for the more mature classes. To validate the labelling of GM *versus* WM classes

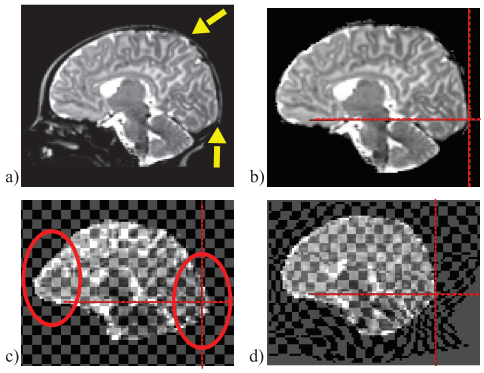

Fig. 1. 6w infant's images : a) T2w-MRI of the brain into the skull. The yellow arrows point towards the direct contact between cerebral tissues and skull. b) T2w-MRI of the brain extracted from the skull. c) Linearly registered qT1 image superimposed on a homogeneous grid. Red circles highlight the main geometrical distortions. d) Non-linearly registered qT1 image superimposed on the associated deformed grid. High deformations appeared corrected (red cross).

resulting from the clustering analysis, we computed Dice indices between these classes and the GM *versus* WM masks obtained through a semi-automatic segmentation obtained from T2w-MRI [11], for the 4 infants used in 2.2.

3. RESULTS

3.1. Distortion correction and multimodal image registration

Figure1 displays a T2w-MRI (**Fig.1b)**), the native qT1 image superimposed on a homogeneous grid (**Fig.1c)**) and the corrected qT1 superimposed on the associated deformed grid (**Fig.1d)**) for a 6w-old infant. The red circles highlight the geometrical distortions in the native qT1 mainly visible in the frontal and occipital regions, which were correctly amended after registration as assessed by visual inspections (see red cross). The deformed grid shows how corrections were locally applied (note the high deformations of the grid in the frontal and occipital regions compared with the hardly affected central brain region).

Figure2 displays the mean Chamfer distances (and their associated standard deviations (SD)) computed between frontal, central (lateral ventricles) and occipital landmarks delineated on $\lambda_{//}$ (resp. on qT1 and qT2) maps and on the T2w images, before (red cross) and after (green circle) the non-linear registration. Before registration, distances were very high for frontal and occipital landmarks (highest values were obtained for qT1 maps). After registration, the mean distances and corresponding SD significantly decreased for the peripheral landmarks, confirming previous visual observations (**Figure1**). On average, the distances computed after the registration were less than 1mm (*i.e.* the anatomical image resolution).

3.2. Clustering analysis

As for the clustering analysis performed on these corrected maps, 4 classes were visually identified in the WM and 3 in the GM. The mean Dice index computed on 4 infants was equal to 0.74 ± 0.02

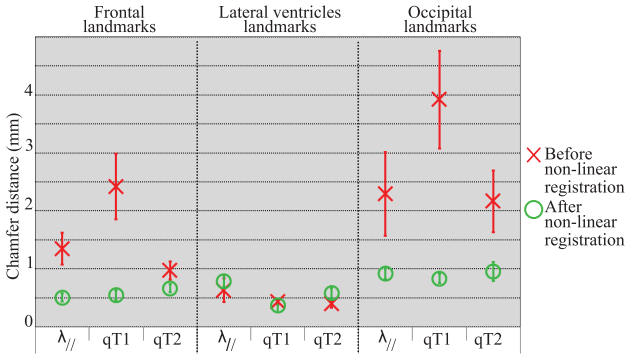

Fig. 2. Mean Chamfer distances and their associated SD computed on 4 infants, between peripheral and central landmarks delineated on $\lambda_{//}$ (resp. on qT1 and qT2) maps and the associated T2w-MRI before (red cross) and after (green circle) the non-linear registration.

when regrouping all GM classes and to 0.63±0.01 when regrouping all WM classes.

Figure3a) shows the WM classes superimposed on T2w-MRI slices for the 4 infants (cf. 2.2). Two main observations suggested that the purple cluster represented the most immature WM, the blue cluster the averagely mature WM, and the green and red clusters the most mature WM : 1) the spatial organization and localization of clusters, in layers from central to peripheral regions, with occipital *versus* frontal differences ; 2) the changes in normalized volumes across the full age range (**Fig.3d)**) : decreasing volumes for the purple and blue clusters, increasing volumes for the green and red clusters. Because of its localization mainly in bundles, we inferred the red class to represent the mature WM compactly organized. The purple class was supposed to represent the immature WM non-compactly organized, being located in the frontal crossroads of the youngest infants (1). Because the same frontal and occipital regions changed from the blue to green clusters with age, WM compactness may not be the main factor providing the distinction between these two clusters. Aside from these interpretations, different maturation patterns were observed across brain regions. The central part of the internal capsule (2) appeared the most mature from the youngest infant. Several regions showed changes in their class labelling with age, suggesting intense maturation over this period : for example the WM region close to the central sulcus (3) and the optic radiations (4). The least mature region in the oldest infants was the frontal crossroads.

Figures3b) and **3c)** illustrate the projection of GM classes voxels on the left inflated inner cortical surfaces of the same infants (lateral and medial views resp.). The normalized volumes (**Fig.3e)**) suggested that the turquoise cluster was the most immature GM (age-related decrease), the yellow cluster was moderately mature GM (inverse-U shape), and the maroon cluster was the most mature GM (age-related increase). Using this scale, the primary cortical regions (central sulcus (5), Heschl's gyrus (6) and calcarine scissure (7)) appeared moderately mature for the youngest infant and became the most mature from 6 weeks of age. Focusing on the lateral surface (**Fig.3b)**), the posterior temporal region (8) close to the superior temporal sulcus seemed moderately mature for the youngest infants and became more mature from 13 weeks of age. The parietal and occipital lobes were mainly classified as immature for the young infants, and also progressively displayed higher maturation with age. The region at the boundary between these two lobes (9) seemed to mature the last. Finally, the frontal lobe maturation followed a similar pattern with a notable delay for the superior region (10). Focusing on the medial surface (**Fig.3c)**), the central grey nuclei (11) seemed to mature early on from the central part to the periphery. The parieto-occipital fissure (12) was moderately mature until 6 weeks of age then become most mature from 13 weeks of age. The middle-posterior cingulum region (13) and the agmydala (14) seemed to display similar maturation patterns.

4. DISCUSSION AND CONCLUSION

This study is a proof of concept to use quantitative mappings based on EPI images to non-invasively study the infant brain maturation within a reasonable acquisition time, and cluster cerebral regions according to their microstructural and maturational properties. The main issue to study such images lies on the distortions inherent to the acquisition. These distortions may be reduced in using specific sequences as the one described in [14]. To exploit our existent database, we chose to correct distortions in post-processing EPI scans through non-linear registration. Quantitative evaluations showed that in average, the variability of the distances computed between the linear-registered quantitative images and associated T2w-MRI depended on the concerned EPI sequence. According to the mean values and their associated SD, the qT1 maps got the highest distortion probably due to the fact that it was the sole sequence not using parallel imaging. The distance values and variability across subjects and across regions significantly decreased after the non-linear registration and got a similar order of magnitude whatever the studied EPI modality (qT1, qT2, DTI). In addition, the mean final distance was less than 1mm (i.e. the anatomical image resolution), which was a required constraint since the cortical thickness is less than 2mm in some regions of the infant brain. This confirmed that the proposed distortion correction was well-adapted to our study.

For the first time, a clustering analysis over a whole infant group was performed and provided partitions of brain tissues that globally agreed with post-mortem studies [1]. On one hand, the progression of maturation within a specific brain region can be easily visualized across infants of different ages. On the other hand, relative advances or delays of maturation across regions, even spatially close, can be observed based on intra-individual analysis. The GM classes showed expected results concerning the maturation of primary regions and of the occipital then frontal lobes. Further non-expected results such as the early maturation of amygdala (similar to the calcarine maturation) were also highlighted. We also observed the well-known progression of WM maturation from central to peripheral regions and from occipital to frontal regions. We initially assumed to separate WM clusters based on differences in compactness properties, in addition to differences in maturational properties, but it did not seem to be possible over this developmental period. Considering either a cohort of infants of equivalent ages, or a higher number of classes will be tested in the future to try to discriminate WM regions based on their intrinsic microstructure (*i.e.* not related to maturation) and refine the GM parcellation. Besides, Dice indices for 4 infants highlighted that some voxels were misclassified in the GM or in the WM, suggesting that performing clustering analyses on GM and on WM separately would refine the results. Unfortunately, anatomical segmentations cannot be easily obtained during the first post-natal year due to the poor and heterogeneous tissue contrast on T1w and T2w-MRI, and manual corrections are required to reliably segment the

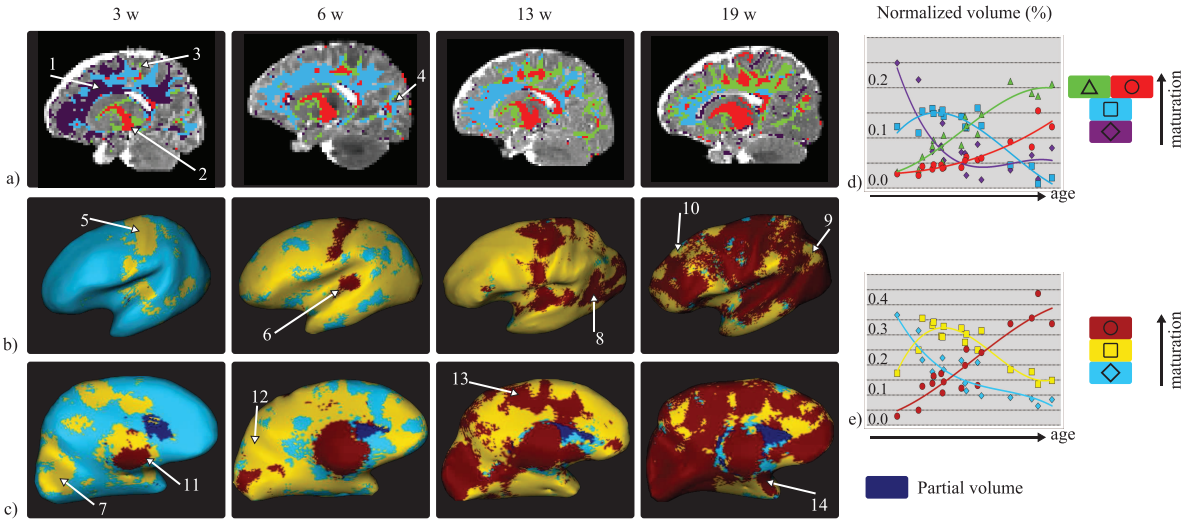

Fig. 3. Clustering analysis results : WM classes superimposed on T2w-MRI slices (a), GM classes projected on left inflated inner cortical surfaces (lateral (b) and medial (c) views). The projection corresponds to the majority of voxel labels computed along an external cylinder (height = 1 voxel, radius = 2 voxels). Normalized volumes of WM and GM classes are on (d) and (e) resp. Anatomical regions highlighted : frontal crossroads (1), internal capsule (2), central sulcus region (3, 5), optic radiations (4), Heschl's gyrus (6), calcarine scissure (7), posterior temporal region (8), boundary region between parietal and occipital lobes (9), superior frontal region (10), central grey nuclei (11), parieto-occipital fissure (12), middle-posterior cingulum region (13), agmydala (14).

maturing GM and WM. Finally, the robustness and information value of the DTI, qT1 and qT2 parameters combination will be considered to evaluate their pertinence for the exploration of GM and WM maturation in the developing brain.

5. REFERENCES

[1] P. Flechsig, *Anatomie des menschlichen Gehirns und Rückenmarks*. 1920.

[2] J. Dubois, G. Dehaene-Lambertz, S. Kulikova, C. Poupon, P. S. Hüppi, and L. Hertz-Pannier, "The early development of brain white matter : A review of imaging studies in fetuses, newborns and infants," *Neuroscience*, vol. 276, pp. 48–71, Sept. 2014.

[3] J. D. Yeatman, B. A. Wandell, and A. A. Mezer, "Lifespan maturation and degeneration of human brain white matter," *Nat Commun*, vol. 5, Sept. 2014.

[4] S. Kulikova, L. Hertz-Pannier, G. Dehaene-Lambertz, A. Buzmakov, C. Poupon, and J. Dubois, "Multi-parametric evaluation of the white matter maturation," *Brain Struct Funct*, pp. 1–16, Sept. 2014.

[5] C. Poupon, J. Dubois, L. Marrakchi, V. Brion, J.-F. Mangin, and F. Poupon, "Real-time EPI t1, t2 and t2* mapping at 3t," (Stockholm, Suede), 2010.

[6] P. Jezzard, "Correction of geometric distortion in fMRI data," *Neuroimage*, vol. 62, pp. 648–651, Aug. 2012.

[7] H. Huang, C. Ceritoglu, X. Li, A. Qiu, M. I. Miller, P. C. van Zijl, and S. Mori, "Correction of b0-susceptibility induced distortion in diffusion-weighted images using large-deformation diffeomorphic metric mapping," *Magn Reson Imaging*, vol. 26, pp. 1294–1302, Nov. 2008.

[8] C. Bhushan, J. Haldar, A. Joshi, and R. Leahy, "Correcting susceptibility-induced distortion in diffusion-weighted MRI using constrained nonrigid registration," in *Signal Information Processing Association Annual Summit and Conference (APSIPA ASC), 2012 Asia-Pacific*, pp. 1–9, Dec. 2012.

[9] F. de Pasquale, A. Cherubini, P. Péran, C. Caltagirone, and U. Sabatini, "Influence of white matter fiber orientation on r2* revealed by MRI segmentation," *J. Magn. Reson. Imaging*, vol. 37, pp. 85–91, Jan. 2013.

[10] D. Duclap, A. Schmitt, B. Lebois, O. Riff, P. Guevara, L. Marrakchi-Kacem, V. Brion, F. Poupon, and C. Poupon, "Connectomist-2.0 : a novel diffusion analysis toolbox for BrainVISA," (Lisbon), Springer, 2012.

[11] F. Leroy, J.-F. Mangin, F. Rousseau, H. Glasel, L. Hertz-Pannier, J. Dubois, and G. Dehaene-Lambertz, "Atlas-free surface reconstruction of the cortical grey-white interface in infants," *PLoS ONE*, vol. 6, p. e27128, Nov. 2011.

[12] D. Rueckert, L. Sonoda, C. Hayes, D. Hill, M. Leach, and D. Hawkes, "Nonrigid registration using free-form deformations : application to breast MR images," *IEEE Transactions on Medical Imaging*, vol. 18, pp. 712–721, Aug. 1999.

[13] C. Kabdebon, F. Leroy, H. Simmonet, M. Perrot, J. Dubois, and G. Dehaene-Lambertz, "Anatomical correlations of the international 10-20 sensor placement system in infants," *Neuroimage*, vol. 99, pp. 342–356, Oct. 2014. WOS :000339860000035.

[14] D. A. Porter and R. M. Heidemann, "High resolution diffusion-weighted imaging using readout-segmented echo-planar imaging, parallel imaging and a two-dimensional navigator-based reacquisition," *Magn Reson Med*, vol. 62, pp. 468–475, Aug. 2009.